

Time-lapse wave-equation migration velocity analysis

Jeffrey Shragge

The University of Western Australia
35 Stirling Highway, Crawley, WA, 6008
jeffrey.shragge@uwa.edu.au

David Lumley

The University of Western Australia
35 Stirling Highway, Crawley, WA, 6008
david.lumley@uwa.edu.au

SUMMARY

Time-lapse analysis of seismic data acquired at different stages of hydrocarbon production or fluid/gas injection has been very successful at capturing detailed reservoir changes (e.g., pressure, saturation, fluid flow). Conventional 4D analysis is performed in the time domain assuming a constant baseline model; however, this procedure becomes difficult when the subsurface is significantly altered by production/injection and large time anomalies and complex 4D coda are recorded. We argue that a more robust 4D analysis procedure in these situations requires iterative wave-equation depth imaging and time-lapse velocity analysis.

Wave-equation depth migration requires accurate knowledge of the velocity field usually obtained by one of two ways. First, data-space methods are where recorded data are matched to those calculated through a background velocity model. Differences between the two datasets are used in tomographic backprojections to generate velocity model updates. Alternatively, image-space methods are where discrepancies between migrated images (non-flat gathers) are backprojected to estimate velocity model updates. These types of approaches are termed migration velocity analysis (MVA).

This abstract focuses on extending 3D wave-equation MVA (WEMVA) approaches to time-lapse velocity analysis. We discuss the differences between 3D and 4D WEMVA inversion goals, and how we leverage the locality of 4D image perturbations to provide high-resolution velocity model updates. We demonstrate the utility of 4D WEMVA analysis in a synthetic CO₂ geosequestration experiment by successfully inverting for a velocity perturbation corresponding to a thin layer (<20m) of injected CO₂ in a typical North Sea reservoir.

Key words: seismic, prestack, inversion, 4D, and velocity.

INTRODUCTION

Time-lapse seismic data acquired at different stages of oil production or steam/CO₂ injection has been very successful at imaging fine-scale changes in petroleum reservoirs (e.g., Greaves and Fulp, 1987; Lumley, 1995; Lumley et al., 1997). The resulting 4D seismic images are interpreted to contain information on changes in reservoir fluid properties [i.e.,

saturation (Anderson et al., 1997; Sonneland et al., 1997) or pressure (Lumley, 1995; Jenkins et al., 1997)] and/or the host rock matrix [i.e., geomechanical compaction (Walls et al., 1998) or fracturing (Johnston et al., 1998)].

4D seismic reservoir monitoring generally is more successfully where the properties of both the reservoir rocks and its pore-space fluids are moderately – but not overly – compressible. 4D seismic analysis in reservoirs where rocks/fluids are too stiff usually leads to weak 4D seismic signals that fall within the 4D noise cone (Lumley, 2010). Conversely, situations where the rocks/fluids are too compliant can cause complex elastic scattering within the reservoir, leading to large time-shift anomalies and hard-to-interpret 4D wavefield coda.

Conventional 4D analysis of moderately compressible rock/fluid systems is performed almost exclusively in the time domain. These analyses make an assumption that the altered (monitor) elastic model can be well represented as a linearised perturbation about a reference (baseline) model. However, the linearisation assumption often is violated where production/injection significantly changes the subsurface. Analogous to the advantages of depth-domain processing relative to time-domain, we argue that for large 4D model changes a robust time-lapse analysis should involve wave-equation depth imaging and a coupled 4D velocity analysis.

Wave-equation depth migration by either one-way (WEM) or two-way (RTM) methods requires accurate knowledge of the velocity field. Most velocity models for depth migration are obtained by one of two approaches. First, one can use *data-space* methods where recorded data are matched to those calculated through a background velocity model. Differences between the two datasets (or residuals) are used in a tomographic back-projection to form a velocity model update. One example of this type of approach is wave-equation tomography (e.g., Gauthier, 1986; Pratt, 1999). Alternatively, one can use *image-space* methods where discrepancies in migrated images (e.g., non-flat gathers) are backprojected to form velocity model updates. These types of approaches are termed migration velocity analysis (MVA) and, when specifically dealing with wave-equation operators, are called wave-equation MVA or WEMVA (e.g., Sava and Biondo, 2004; Albertin, 2006; Girard and Vasconcelos, 2010).

This abstract focuses on applying 3D WEMVA approaches to the problem of time-lapse velocity analysis. We begin with a brief discussion of the WEMVA methodology, and outline the key differences between 3D and 4D approaches. We present a realistic synthetic 4D experiment drawn from – but not identical to – observations from the Sleipner CO₂ injection project located offshore in the Norwegian North Sea. Finally,

we present imaging and 4D WEMVA inversion results that demonstrate the utility of the method.

TIME-LAPSE WEMVA

WEMVA is a fairly well established approach for 3D seismic velocity analysis in complex geology (Biondi and Sava, 1999; Sava and Biondi, 2004; Shen et al., 2006). Herein, we follow a WEMVA procedure based on that discussed in Sava and Vlad (2008). Because these authors provide an excellent procedural overview, we refrain from detailing conventional 3D WEMVA theory. Rather, we briefly summarize the goals of the WEMVA technique and provide some of the key differences between the 3D and 4D approaches.

The key idea in WEMVA is that a perturbation in the velocity model will cause a perturbation in a migration image (or vice-versa). These two spaces are linked by the source and receiver wavefields that are “carriers of information” that can be used in acoustic wavefield tomographic backprojections to transfer information between the velocity and image spaces. The forward WEMVA operator describes how a velocity perturbation (Δv) will generate perturbed source/receiver wavefields (ΔW) that in turn cause image-space perturbations (ΔI). Symbolically, this may be written as:

$$\Delta v \Rightarrow \Delta W \Rightarrow \Delta I. \quad (1)$$

The adjoint WEMVA operator describes how information flows in the opposite sense from image to velocity model:

$$\Delta I \Rightarrow \Delta W \Rightarrow \Delta v. \quad (2)$$

That is, an image-space perturbation causes source/receiver wavefield perturbations that lead to an altered velocity model. Thus, the WEMVA inversion goal is to find the Δv that optimally explains the observed ΔI .

4D WEMVA differs from the 3D approaches in two key respects. The first difference is the WEMVA minimization goal. 3D WEMVA uses the difference between an image constructed from field data and an idealized conceptual version of what it should be (i.e., flat angle gathers or focused differential semblance). The 3D WEMVA goal is to alter the velocity model such that the subsequent migration image becomes closer to the idealized version (i.e., has flatter angle gathers or better focused differential semblance panels). In contrast, 4D WEMVA uses differences between images constructed from two *field* datasets. The 4D WEMVA goal is to alter the velocity model such that the two images optimally match, even if individual image gathers themselves are not optimized in the conventional sense (i.e., contain residual gather curvature or sub-optimal focusing).

A second difference is that true 4D model alterations usually are spatial localized because production/injection-induced changes largely remain localized within – and do not spread far beyond – the reservoir. Being a tomographic technique, 3D WEMVA backprojections tend to spread the estimated velocity perturbations throughout the entire velocity model. However, we can set up the WEMVA inversion procedure to force velocity updates to be local through the use of spatial weight masks. This enforces the idea that 4D perturbations are due to local changes in pressure and saturation or geomechanical alteration such as compaction and extension. (Understanding which underlying mechanism(s) is responsible for the changes is another matter.)

SYNTHETIC EXPERIMENT

To demonstrate the utility of 4D WEMVA, we present a synthetic experiment of CO₂ injection loosely based on observations from the Sleipner CO₂ sequestration experiment conducted in the Norwegian North Sea. The top panel of Figure 1 shows the baseline P-wave velocity model prior to CO₂ injection. The middle panel shows our monitor model of P-wave velocity after a “few years” of CO₂ injection. We model a scenario where the injected gas has spread out in a thin layer ($\Delta z_{\text{true}} < 20\text{m}$ thick) over a 1.5km zone and causes a 25% drop in P-wave velocity ($\Delta v_p = -0.4 \text{ km/s}$) between the baseline and monitor surveys. These changes are broadly consistent with other numerical Sleipner CO₂ flow simulation models (e.g., Lumley et al, 2009). The S-wave and density models (not shown) change 0% and 5%, respectively, within in the perturbed zone. The bottom panel in Figure 1 represents the 4D velocity perturbation that we are trying to recover through the 4D WEMVA procedure.

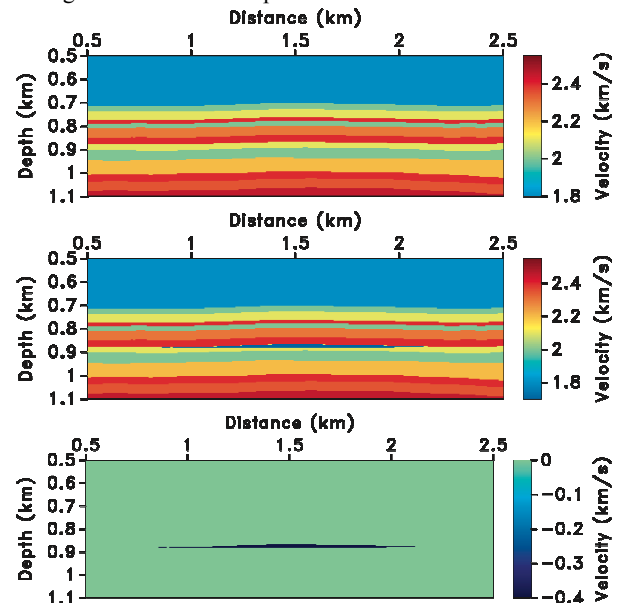


Figure 1. Velocity models used for generating the elastic finite difference data. Top: Baseline P-wave velocity model. Middle: Monitor P-wave velocity model above after CO₂ injection. Bottom panel: Velocity difference between top and middle panels showing a $\Delta v = -0.4 \text{ km/s}$ drop due to the presence of CO₂.

We used an isotropic elastic finite-difference modeling code on the two elastic model sets to generate baseline and monitor data sets for experimentation. We assumed fixed acquisition geometry (equivalent to an ocean-bottom cable survey) with receivers located every 4m between horizontal distances of 0-2.8km. We modeled a total of 144 shots equally spaced at a 16m interval along the receiver line. The central frequency of the wavelet was 45Hz with a high-cut filter applied at 100Hz.

Figure 2 presents two shot records from the baseline (left panel) and monitor (middle panel) data volumes for a 1.5km source point. The right panel shows the 4D data difference. Note that even though we altered only one layer, we observe significant changes in the 4D wavefield coda. In this abstract, we argue that the presence of this wavefield complexity renders 4D time-domain interpretation very difficult, and necessitates depth-domain processing approaches that can help unravel wavefield complexity.

We input the baseline and monitor data sets into a one-way wave-equation depth migration algorithm using the (slightly smoothed) P-wave velocity models shown in Figure 1. For reasons discussed below, we aggressively bandpass filtered (30Hz high-cut) the data prior to migration to generate the low frequency images shown in Figure 3. The top panel shows the baseline imaging experiment constructed from the baseline data and a baseline migration velocity. The middle panel shows the monitor image constructed from the monitor data also using the baseline migration velocity model. We see significant reflectivity changes between these two images due to the altered CO₂ layer. This change is better illustrated in the difference image (bottom panel).

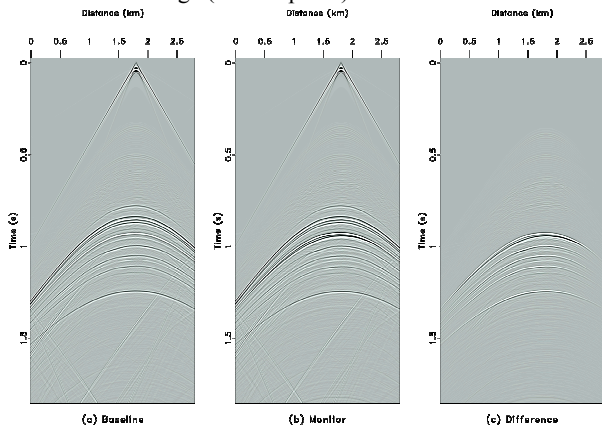


Figure 2. Shot-gather examples from the elastic finite difference data volumes (vertical component) computed through models shown in Figure 1. Shots were extracted from data volumes at 1.5km. Left: Baseline shot record. Middle: Monitor shot record. Right: Difference between baseline and monitor shot records.

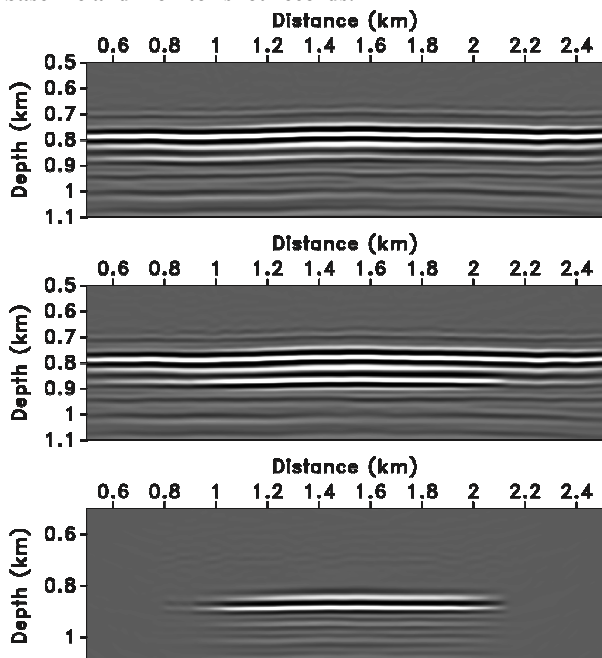


Figure 3. Image differences for the various data sets. Top: Baseline data set migrated with the (correct) baseline velocity model. Middle: Monitor data set migrated with the (incorrect) baseline velocity model. Bottom: Image difference between top and middle panels representing the time-lapse perturbation used for 4D WEMVA inversion.

4D WEMVA INVERSION

The 4D WEMVA goal of the synthetic experiment is to estimate the velocity perturbation that gave rise to the computed image perturbation (Figure 3, bottom panel). We applied the two procedural changes to the 3D WEMVA algorithm detailed in Sava and Vlad (2008).

First, during experimental testing we found that using the full frequency band (3-100Hz) led to cycle skipping in difference images and non-convergence of the 4D WEMVA inversion. We applied a 30Hz high-cut filter to the data prior to migration that, though generated lower frequency images, resulted in image differences free from cycle skipping. We note that this restriction could be relaxed to a higher frequency band in later iterations when the inversion arc closer to convergence and higher frequency image differences are less prone to cycle skipping.

A second 4D WEMVA procedural difference is that we forced the imaged perturbations to be localised velocity changes. We accomplished this by using spatial weighting operators constructed directly from the 4D difference image. Figure 4 presents the spatial weight mask used in the WEMVA inversions. We constructed this mask by taking the envelope of the difference image and iteratively applying a 12-point smoothing filter in both directions. This retains a relative weighting between low and high amplitude events and forces the inversion to fit the larger perturbations first.

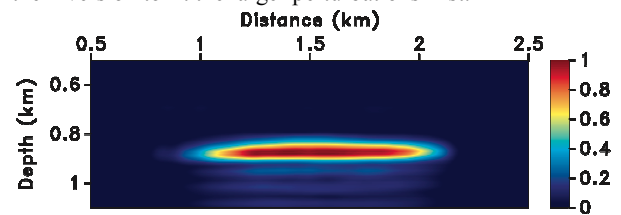


Figure 4. Model mask generated by taking envelope of difference image and applying a smoothing filter of 12x12 pixels a total of ten times.

Figure 5 presents the results of applying the adjoint 4D WEMVA operator to the input image perturbation using the mask shown in Figure 4. Results are presented in slowness rather than velocity. The recovered perturbation is located in the correct position and has the correct polarity (i.e., a negative velocity perturbation corresponds to a positive slowness change). Note that the slowness scale bar is arbitrary because we have not used inversion to fix the true scaling.

The middle panel shows the inversion result after the 8th iteration. The algorithm recovered a maximum slowness perturbation, Δs_{inv} , roughly half of the true result, Δs_{true} . However, the thickness of inverted perturbation, Δz_{inv} , is roughly twice that of the true result (bottom panel). This observation is consistent with an “uncertainty” relationship that marks a trade-off between perturbation magnitude and its compactness: $\Delta s_{true}\Delta z_{true} \approx \Delta s_{inv}\Delta z_{inv}$. Future tests will determine whether we can improve on this result by using a higher seismic frequency band for inversion, or whether it is a fundamental limit due to using approximate physics (i.e. acoustic versus elastic). Finally, Figure 6 shows that the WEMVA analysis has converged after eight iterations with the inverted perturbation accounting for > 99% of residual energy.

CONCLUSIONS

We present an application of the 4D WEMVA approach to two synthetic data sets modelled after field Sleipner CO₂ injection experiment. By using a lower frequency band than used in conventional imaging and incorporating spatial weight masks to localise slowness perturbations, we were able to invert a time-lapse difference image for the corresponding slowness perturbation. This success should motivate the use of 4D WEMVA in field data trials.

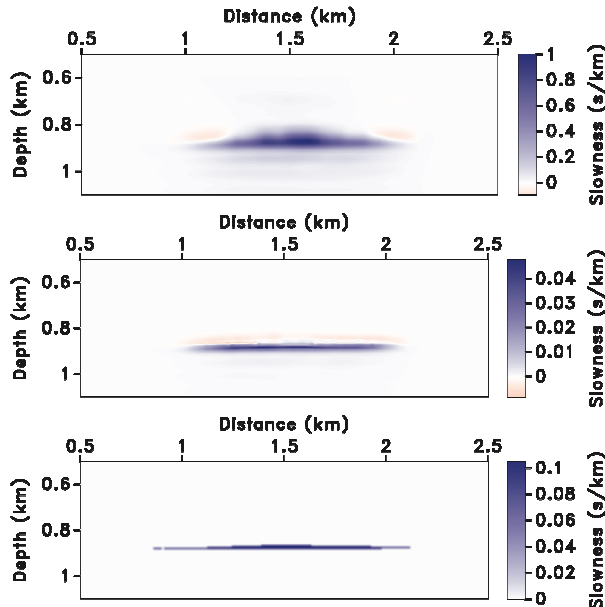


Figure 5. Slowness perturbations. Top: Adjoint WEMVA operator results with an arbitrary slowness scale. Middle: 4D WEMVA inversion results after the 8th iteration. Bottom: True 4D slowness perturbation.

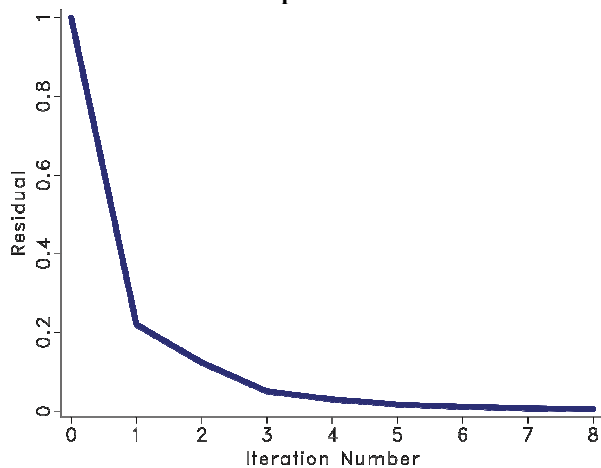


Figure 6. L₂ norm residuals for the WEMVA inversion showing quick convergence after eight iterations.

ACKNOWLEDGMENTS

This research was partly funded by the sponsors of the UWA:RM consortium. We thank Paul Sava and Tony Yang for assistance with the 3D WEMVA codes. Shragge acknowledges WAERA for Research Fellowship support.

REFERENCES

Albertin, U., P. Sava, J. Etgen, and M. Maharramov, 2006, Adjoint wave-equation velocity analysis: SEG Expanded Abstracts, **25**, 3009-3013.

Anderson, R. N., A. Boulanger, W. He, L. Xu, P. B. Flemings, T. D. Burkhart, and A. R. Hoover, 1997, 4-D time-lapse seismic monitoring in the south Timbalier 295 field, Gulf of Mexico: SEG Expanded Abstracts, **18**, 868-871.

Biondi, B., and P. Sava, 1999, Wave-equation migration velocity analysis: SEG Expanded Abstracts, **20**, 1723-1726.

Gauthier, O., J. Virieux, and A. Tarantola, 1986, Two-dimensional nonlinear inversion of seismic waveforms - Numerical results: Geophysics, **51**, 1387-1403.

Girard, A., and I. Vasconcelos, 2010, Image-domain time-lapse inversion with extended images, SEG Expanded Abstracts, **29**, 4200-4203.

Greaves, R. J., T. J. and Fulp, 1987, Three-dimensional seismic monitoring of an enhanced oil recovery process: Geophysics, **52**, 1175-1187.

Jenkins, S. D., M. W. Waite, and M. F. Bee, 1997, Time-lapse monitoring of the Duri steamflood: A pilot and case study: The Leading Edge, **16**, 1267-1273.

Johnston, D. H., R. S. McKenny, J. Verbeek, and J. Almond, 1998, Time-lapse seismic analysis of Fulmar Field: The Leading Edge, **17**, 1420-1428.

Lumley, D. E., 1995, Seismic time-lapse monitoring of subsurface fluid flow: Ph.D. thesis, Stanford University.

Lumley, D. E., R. A. Behren, and Z. Wang, 1997, Assessing the technical risk of a 4-D seismic project: The Leading Edge, **16**, 1287-1291.

Lumley, D.E., D. Adams, R. Wright, D. Markus, and S. Cole, 2008, Seismic monitoring of CO₂ geo-sequestration: realistic capabilities and limitations: SEG Expanded Abstracts, **27**, 2841-2845.

Pratt, R. G., 1999, Seismic waveform inversion in the frequency domain, Part 1: Theory and verification in a physical scale model: Geophysics, **64**, 888-901.

Sava, P., and B. Biondi, 2004, Wave-equation migration velocity analysis - I: Theory: Geophysical Prospecting, **52**, 593-606.

Sava, P., and I. Vlad, 2008, Numeric implementation of wave-equation migration velocity analysis operators: Geophysics, **73**, no 5, VE145-VE159.

Shen, P., W. Symes, S. Morton, and H. Calandra, 2005, Differential semblance velocity analysis via shot profile migration: SEG Expanded Abstracts, **24**, 2249-2252.

Sirgue, L., and R. Pratt, 2004, Efficient waveform inversion and imaging: A strategy for selecting temporal frequencies: Geophysics, **69**, 231-24.

Walls, J. D., J. Dvorkin, and B. A. Smith, 1998, Modeling seismic velocity in Ekofisk Chalk: SEG Expanded Abstracts, **19**, 1016-1019.

